Journal of Alloys and Compounds 509 (2011) 1226–1230

Contents lists available at ScienceDirect

Journal of Alloys and Compounds

journal homepage: www.elsevier.com/locate/jallcom

Preparation and thermal conductivities of $Gd_2Ce_2O_7$ and $(Gd_{0.9}Ca_{0.1})_2Ce_2O_{6.9}$ ceramics for thermal barrier coatings

Hongsong Zhang[a,c,*], Suran Liao[b], Xudan Dang[a], Shaokang Guan[c], Zheng Zhang[a]

[a] Department of Mechanical Engineering, Henan Institute of Engineering, Zhengzhou 450007, China
[b] Department of Materials and Chemistry, Henan Institute of Engineering, Zhengzhou 450007, China
[c] School of Materials Science and Engineering, Zhengzhou University, Zhengzhou 450002, China

ARTICLE INFO

Article history:
Received 13 July 2010
Received in revised form
26 September 2010
Accepted 28 September 2010
Available online 8 October 2010

Keywords:
Cerium oxides
Thermal conductivity
Phonon scattering
Thermal barrier coatings

ABSTRACT

Two kinds of rare earth cerium oxides $Gd_2Ce_2O_7$ and $(Gd_{0.9}Ca_{0.1})_2Ce_2O_{6.9}$ were prepared by solid state reaction method at 1600 °C for 10 h. The phase compositions, microstructures, and their thermal conductivities of these materials were investigated. XRD results revealed that single phase $Gd_2Ce_2O_7$ and $(Gd_{0.9}Ca_{0.1})_2Ce_2O_{6.9}$ with fluorite structure were synthesized. Results of SEM and EDS showed that the microstructures of these materials were dense and no other phases existed among grains. Because of phonon scattering resulted by the oxygen vacancies and difference in atomic mass between substitutional atoms and host atoms, thermal conductivities of $Gd_2Ce_2O_7$ and $(Gd_{0.9}Ca_{0.1})_2Ce_2O_{6.9}$ are lower than that of 8YSZ at 800 °C, and thermal conductivity of $(Gd_{0.9}Ca_{0.1})_2Ce_2O_{6.9}$ is lower than that of $Gd_2Ce_2O_7$. These results imply the $Gd_2Ce_2O_7$ and $(Gd_{0.9}Ca_{0.1})_2Ce_2O_{6.9}$ can be used as novel candidate materials for thermal barrier coatings in the future.

1. Introduction

Thermal barrier coatings (TBCs) are widely used in both gas and diesel turbine engines to protect hot-section metallic components from corrosion and oxidation at elevated temperatures, and to enhance component life and performance [1,2]. Zirconate-based ceramic TBCs have attracted increasing attention for advanced engine applications due to their ability to provide thermal insulation for hot-section components. Some important requirements for good TBCs are low thermal conductivity, high thermal expansion coefficient, high-phase stability, and low sintering rate at elevated temperatures [3]. However, zirconate-based ceramic is limited to applications below 1200 °C due to its sintering resistance and phase structure stability during long-term service [3,4]. In order to further increase the operating efficiency, it is urgently needed to develop new thermal oxides with a significantly lower thermal conductivity than YSZ for further improvements in engine's performance to increase gas inlet temperatures to 1650 °C or higher. Two important groups of candidate materials, one based on the co-doped of yttria-stabilized zirconia (YSZ) with one or more metal oxides and the other on the rare-earth zirconate ceramics, have been developed for advanced gas-turbine engines, which are intended to operate at temperatures as high as possible [5,6].

The rare earth zirconates with general formula $Ln_2Zr_2O_7$ (Ln = rare earth elements) with pyrochlore structures or defect fluorite-type structures, show promising thermophysical properties. The thermal conductivities of $Ln_2Zr_2O_7$ (Ln = La, Nd, Sm, Eu, Gd, Dy, etc.) ceramics range from 1.1 to 1.2 W/m K, which are lower than that of YSZ [7–10]. Because of their promising thermophysical properties, efforts have also been made to investigate the co-doped $Ln_2Zr_2O_7$ ceramics with one or more metal oxides in recent years [10–14]. However, their have relative low coefficients of thermal expansion (CTEs) resulting in high thermal stress in TBC applications, which is harmful for TBC's performance [15–17].

It is well known that CeO_2 has high thermal expansion coefficient because of its lower melting point compared to ZrO_2, which indicates that the thermal expansion coefficient may be improved by the substitution of CeO_2 for ZrO_2. That is, the $Ln_2Ce_2O_7$ (Ln represents rare earth elements, too) ceramics may have larger thermal expansion coefficients than corresponding $Ln_2Zr_2O_7$ ceramics. Thermophysical properties of $La_2Ce_2O_7$ and $Nd_2Ce_2O_7$ ceramics have been reported by C.X. Qiang, etc. Results show that $La_2Ce_2O_7$ and $Nd_2Ce_2O_7$ have lower thermal conductivities than YSZ, while their thermal expansion coefficients are higher than those of $La_2Zr_2O_7$ and $Nd_2Zr_2O_7$ ceramics. Moreover, they also show better phase stability at high temperatures [18,19]. These properties indicate sufficiently that $La_2Ce_2O_7$ and $Nd_2Ce_2O_7$ can be explored as new thermal barrier coating

* Corresponding author at: Henan Institute of Engineering, Mechanical and Electrical Engineering, Tongbai Road, No. 62, Zheng Zhou City, Henan Province 450007, China. Tel.: +86 0371 62508765.
E-mail addresses: zhs761128@163.com, zhsandchen@126.com (H. Zhang).

0925-8388/$ – see front matter © 2010 Elsevier B.V. All rights reserved.
doi:10.1016/j.jallcom.2010.09.196

materials. Patwe's research results show that thermal expansion coefficient of $Gd_2Ce_2O_7$ is 13.8×10^{-6}/K [20], which is greater than that of $Gd_2Zr_2O_7$ (11.6×10^{-6}/K). However, thermal conductivity of $Gd_2Ce_2O_7$ has not been reported up to now. In order to confirm whether $Gd_2Ce_2O_7$ can be explored as new candidate material for thermal barrier coating materials, $Gd_2Ce_2O_7$ ceramic samples were synthesized by solid reaction and the microstructure and thermal conductivity of this ceramic were examined in this research. Because the doption of substitutional ions can increase phonon scattering which is useful to reducing thermal conductivity of ceramic compounds, and there is no research report about thermophysical properties of rare earth cerium oxides up to now. So, the properties of $(Gd_{0.9}Ca_{0.1})_2Ce_2O_{6.9}$ were investigated at the same time, too.

2. Experimental

Samples of $Gd_2Ce_2O_7$ and $(Gd_{0.9}Ca_{0.1})_2Ce_2O_{6.9}$ were synthesized by means of the solid state reaction method, using CeO_2 (Rare-Chem Hi-Tech Co., LTD, purity ≥99.99), Gd_2O_3 (Rare-Chem Hi-Tech, Co., LTD, purity ≥99.99%) and CaO (purity ≥99.99%) as the starting materials. After mixing the constituents thoroughly in an agate mortar, the powder mixtures were calcined at 800 °C for 5 h in air. Then the powders were uniaxially cold pressed into pellets, and the pellets were placed on cerium tiles and sintered at 1600 °C for 10 h. The pellets were subsequently cooled in air from 1600 °C in the end.

Phase composition analysis of the synthesized samples were determined by X-Ray diffractometry (XRD, X'Pert PRD MPD Holand) with Ni filtered CuKα radiation (0.1542 nm) at the scanning rate of 4°/min. The morphology of fractured cross-sections was analyzed using scanning electron microscope (SEM, HITACHI S-4800).

The thermal diffusivities (λ) of synthesized samples were measured using laser-flash method (Model FlashLine™ 3000, Anter, USA) in the range between ambient and 800 °C in an argon atmosphere. The sample dimension for thermal diffusivity measurement was about 12.7 mm in diameter and about 1 mm in thickness. Before thermal diffusivity measurement, both the front and back faces of the samples were coated with a thin layer of graphite. These coatings were done to prevent direct transmission of laser beam through the translucent specimens. The thermal diffusivity measurement of the specimens was carried out three times at 200 °C, 400 °C, 600 °C and 800 °C, respectively. The specific heat capacity (C_p) as a function of temperature was calculated from the chemical composition of $Gd_2Ce_2O_7$ and $(Gd_{0.9}Ca_{0.1})_2Ce_2O_{6.9}$ and the heat capacity data of the constituent oxides, in conjunction with the Neumann–Kopp rule [21,22]. The thermal conductivities (k) of the specimens were calculated by Eq. (1) with specific heat capacity (C_p), density (ρ) and thermal diffusivity (λ).

$$k = \lambda \cdot \rho \cdot C_P \quad (1)$$

Because the sintered specimens were not full dense, the measured values of thermal conductivities were modified for the actual value k_0 using Eq. (2), where ϕ is the fractional porosity and the coefficient 4/3 is used to eliminate the effect of porosity on actual thermal conductivity.

$$\frac{k}{k_0} = 1 - \frac{4}{3}\phi \quad (2)$$

3. Results and discussion

3.1. Phase compositions

The XRD patterns of $Gd_2Ce_2O_7$, $(Gd_{0.9}Ca_{0.1})_2Ce_2O_{6.9}$ and $Gd_2Zr_2O_7$ prepared by solid reaction are shown in Fig. 1. Fig. 1 indicates that the XRD patterns of the prepared ceramics are coincident with the standard spectrum of $Gd_2Ce_2O_7$ and no other phases exist in these products. It can be seen that the XRD patterns of $Gd_2Ce_2O_7$ and $(Gd_{0.9}Ca_{0.1})_2Ce_2O_{6.9}$ are similar to that of $Gd_2Zr_2O_7$. But $Gd_2Zr_2O_7$ has two additional weak peaks between $2\theta = 40°$ and 50°. These two peaks can help us to distinguish the fluorite and pyrochlore structures [18,19]. It can be concluded that pure $Gd_2Ce_2O_7$ and $(Gd_{0.9}Ca_{0.1})_2Ce_2O_{6.9}$ ceramics with fluorite structure were synthesized in this research. The early research results revealed that the ionic radius ratio, $RR = (r_A^{3+}/r_B^{4+})$ of oxides with the type of $A^{3+}{}_2B^{4+}{}_2O_7$, and the oxygen parameter (x) govern the formation and phase stability of these oxides. Pyrochlore oxides can form for RR = 1.46–1.78 at one atmosphere, and fluorite oxides will form if RR is lower than 1.46 [23]. The RR of $Gd_2Ce_2O_7$ and $(Gd_{0.9}Ca_{0.1})_2Ce_2O_{6.9}$ ceramics are only 1.144 and 1.132, respectively, which also indicate that these two ceramics have fluorite structure. The lattice constants of $Gd_2Ce_2O_7$ and $(Gd_{0.9}Ca_{0.1})_2Ce_2O_{6.9}$ are 1.043 and 1.091 which are calculated according to their XRD patterns. The lattice constant and the XRD pattern of $(Gd_{0.9}Ca_{0.1})_2Ce_2O_{6.9}$ in Fig. 1show that Ca^{2+} ions have been dissolved in the $Gd_2Ce_2O_7$ through substitution.

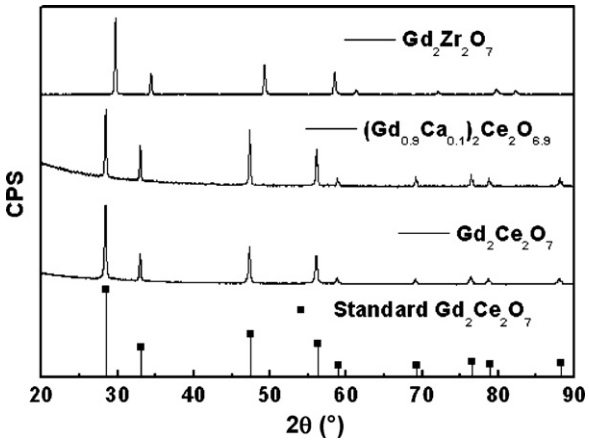

Fig. 1. XRD patterns of synthesized ceramics.

Table 1
Relative densities of $Gd_2Ce_2O_7$ and $(Gd_{0.9}Ca_{0.1})_2Ce_2O_{6.9}$ ceramics.

Ceramic block	$Gd_2Ce_2O_7$	$(Gd_{0.9}Ca_{0.1})_2Ce_2O_{6.9}$
Density (g/cm³)	7.295	6.586
Relative density (%)	98.5	91.9

3.2. Microstructure

Fig. 2 shows the typical microstructures of $Gd_2Ce_2O_7$ and $(Gd_{0.9}Ca_{0.1})_2Ce_2O_{6.9}$ prepared by solid reaction synthesis. As can be seen from Fig. 2, the microstructures of the synthesized products are very similar. Their microstructures are very dense. The densities of these samples determined by Archimedes method with an immersion medium of deionized water are shown in Table 1. It can be seen from Table 1 that, the relative densities of $Gd_2Ce_2O_7$ and $(Gd_{0.9}Ca_{0.1})_2Ce_2O_{6.9}$ ceramic samples are 98.5% and 91.9%, respectively. The interfaces between particles were very clean and no other interphases or unreacted oxides existed in the interfaces, which is confirmed by the corresponding EDS analysis as shown in Fig. 3 [24]. The EDS microanalysis pattern in Fig. 3 performed on selected areas revealed the presence of mixed oxide phases for Gd–Ce–O and Gd–Ca–Ce–O. The results of element atomic ratios of these prepared products are displayed in Table 2. As can be seen from Table 2 that the element atomic ratios are consistent with the stoichiometry ratios making up to $Gd_2Ce_2O_7$ and $(Gd_{0.9}Ca_{0.1})_2Ce_2O_{6.9}$ respectively. Results of EDS analysis displayed in Fig. 3(b) and Table 2 also imply that Ca^{2+} ions have been dissolved in the $Gd_2Ce_2O_7$ through substitution, which is consistent with XRD pattern of $(Gd_{0.9}Ca_{0.1})_2Ce_2O_{6.9}$.

Table 2
Element atomic ratio of $Gd_2Ce_2O_7$ and $(Gd_{0.9}Ca_{0.1})_2Ce_2O_{6.9}$ ceramics.

Sample	Element atomic%				
	Gd	Ce	O	Ca	Totals
$Gd_2Ce_2O_7$	16.3	16.77	66.93	–	100
$(Gd_{0.9}Ca_{0.1})_2Ce_2O_7$	14.2	17.51	67.25	1.22	100

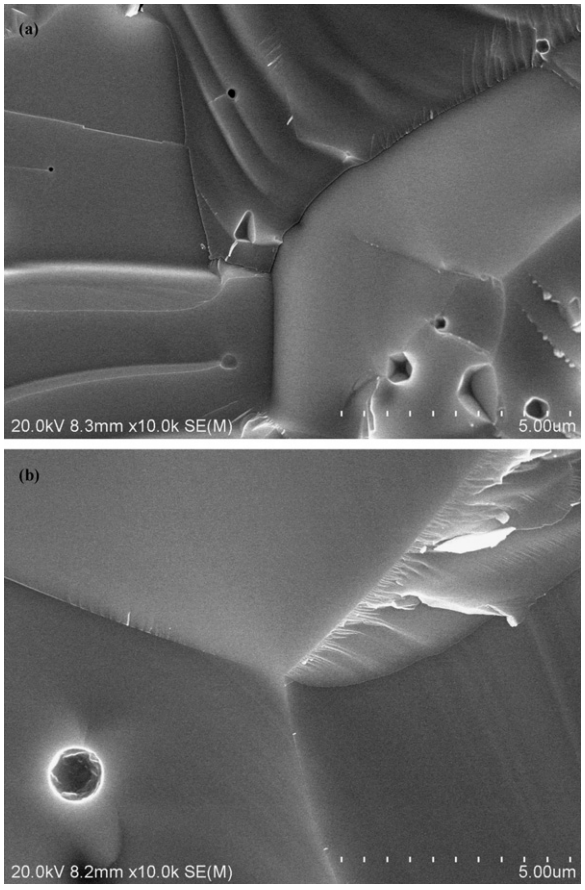

Fig. 2. Microstructure of ceramic samples (a) $Gd_2Ce_2O_7$ (b) $(Gd_{0.9}Ce_{0.1})_2Ce_2O_{6.9}$.

3.3. Thermal conductivities

The specific heat capacities of $Gd_2Ce_2O_7$ and $(Gd_{0.9}Ca_{0.1})_2Ce_2O_{6.9}$ for various temperatures increase with the temperature increase in the range between ambient and 1000 °C, which is plotted in Fig. 4. The specific heat capacities of these ceramics can be fitted as the following equations in this temperature range.

$$C_p(Gd_2Ce_2O_7) = 0.3652 + 0.0001 \times T - 56.1143 \times T^{-2} \quad (3)$$

$$C_p(Gd_{0.18}Ca_{0.2}Ce_2O_{6.9}) = 0.37486 + 0.0001 \times T - 81.72533 \times T^{-2} \quad (4)$$

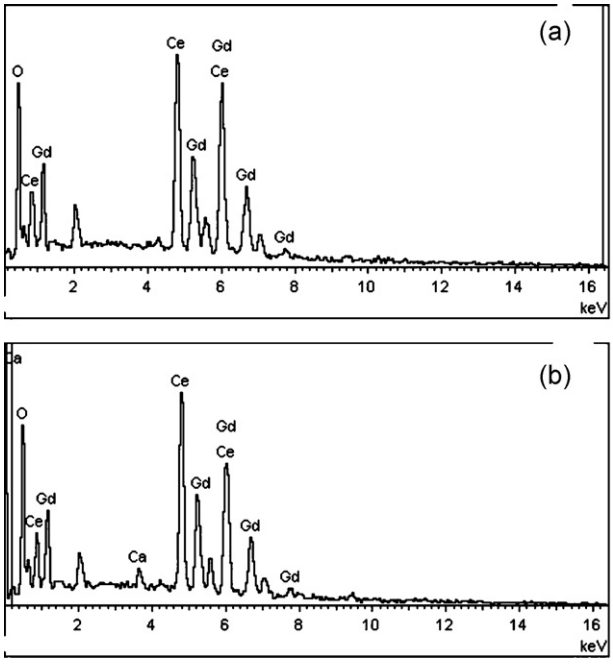

Fig. 3. EDS analysis results of ceramic samples (a) $Gd_2Ce_2O_7$ (b) $(Gd_{0.9}Ca_{0.1})_2Ce_2O_{6.9}$.

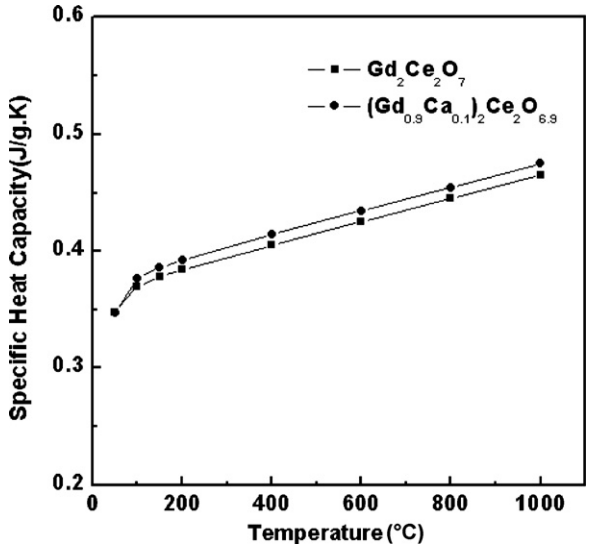

Fig. 4. Specific heat capacities of $Gd_2Ce_2O_7$ and $(Gd_{0.9}Ca_{0.1})_2Ce_2O_{6.9}$ ceramic materials at different temperatures.

The thermal diffusivities of $Gd_2Ce_2O_7$ and $(Gd_{0.9}Ca_{0.1})_2Ce_2O_{6.9}$ ceramics at different temperatures are presented in Fig. 5. It can be seen from Fig. 5 that thermal diffusivities of these ceramic materials decrease with the temperature increase in the range between 200 °C and 800 °C. The T^{-1}-dependence of diffusivities for these two ceramic materials suggests a dominant phonon conduction behavior, which is common for most of the polycrystalline materials [25].

Fig. 6 indicates the thermal conductivities of $Gd_2Ce_2O_7$ and $(Gd_{0.9}Ca_{0.1})_2Ce_2O_{6.9}$ as a function of temperature. Thermal conduc-

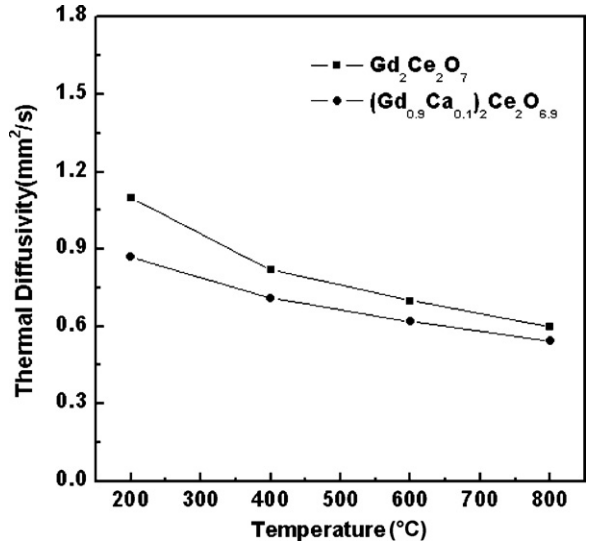

Fig. 5. Temperature dependence of thermal diffusivities of $Gd_2Ce_2O_7$ and $(Gd_{0.9}Ca_{0.1})_2Ce_2O_{6.9}$ ceramic materials.

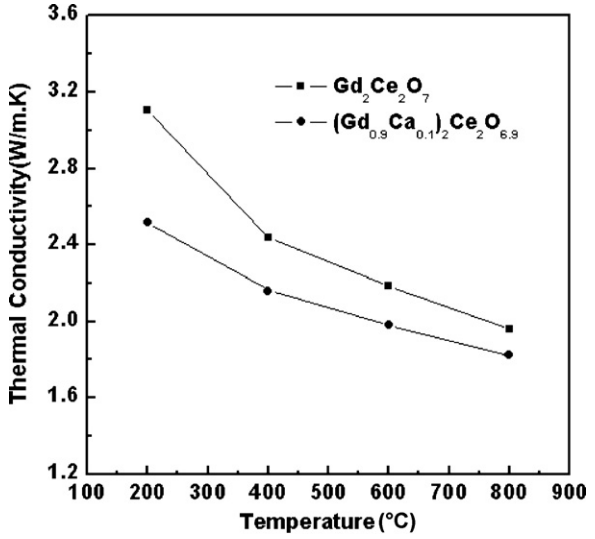

Fig. 6. Thermal conductivities of $Gd_2Ce_2O_7$ and $(Gd_{0.9}Ca_{0.1})_2Ce_2O_{6.9}$ ceramic materials for various temperatures.

tivity of $Gd_2Ce_2O_7$ decreased from 3.10 W/m K to 1.96 W/m K in this temperature of 200–800 °C, and the value of thermal conductivity of $(Gd_{0.9}Ca_{0.1})_2Ce_2O_{6.9}$ decreased from 2.52 W/m K to 1.87 W/m K. These results are almost lower 10% and 20% than that of YSZ (about 2.15 W/m K at 800 °C [19]), respectively. It is well known that the thermal conductivity of CeO_2 is higher than that of YSZ at temperatures below 1300 °C (2.77 W/m K at 1000 °C).

To rationalize these results, the theory of heat conduction is considered. In electrical insulating solids, the thermal conductivity results from lattice vibrations or by radiation. The contribution to thermal conductivity from lattice vibration (k), the quanta of which are known as phonons, is given by:

$$k = \frac{1}{3} C_v l_p \rho v \tag{5}$$

where C_v is the specific heat capacity, ρ is the density, v is the phonon velocity and l_p is the mean free path for scattering of phonons.

To reduce the intrinsic thermal conductivity of a material, reductions in the specific heat capacity, phonon velocity, mean free path, or density are needed. The specific heat capacity at constant volume (C_v) for any system is constant at a value of $3kbN \approx 25\,J\,K^{-1}\,mol^{-1}$ above the Debye temperature. The value of v is related with elastic ratio (E) and density (ρ), the effect of temperature on the elastic ratio and density is not obvious, so the value of v may be also regarded as a constant approximately. Consequently, the value of the thermal conductivity (k) is mainly decided by the law that the mean free path of phonon decreases with increasing temperature among most polycrystalline ceramic materials. In real crystal structures scattering of phonons occurs when they interact with lattice imperfections in the ideal lattice. Such imperfections include vacancies, dislocations, grain boundaries, atoms of different masses and other phonons. Ions and atoms of different ionic radius may also scatter phonons by locally distorting the bond length and thus, introducing elastic strain fields into the lattice. The effects caused by such imperfections can be quantified through their influence on the phonon mean free path (l_p). This approach has been used by many workers, for which the phonon mean free path is defined by:

$$\frac{1}{l_p} = \frac{1}{l_i} + \frac{1}{l_{vac}} + \frac{1}{l_{gb}} + \frac{1}{l_{strain}} \tag{6}$$

where l_i, l_{vac}, l_{gb} and l_{strain} are the contributions to the mean path due to interstitials, vacancies, grain boundaries and lattice strain, respectively [26].

The decrease of the thermal conductivity due to the phonon scattering at grain boundaries is not expected in the case of the ceramic materials investigated here. For a significant decrease in the high-temperature range, the average grain size has to be in the nanometer region, whereas the current specimens have grain size in the micrometer range. Also, radiation heat transfer can be neglected because the maximum temperature considered here is only 800 °C. Thus, the decrease in the phonon conductivity is assumed to result solely from phonon scattering by point defect. The two types of point defects expected in the materials studied here are substitutional gadolinium solute cation replacing cerium and the corresponding oxygen vacancies created by the substitution of tetravalent cerium by a trivalent gadolinium cation. The defect chemistry due to co-doping can be represented using the Kröger–Vink notation by the following equation,

$$Gd_2O_3 \xrightarrow{CeO_2} 2Gd'_{Ce} + V''_o + 3O^x_o \tag{7}$$

where Gd'_{Ce} represents an Gd^{3+} cation that occupies a Ce^{4+} cation site (single negative charge), V''_o is a doubly charged (positive) oxygen vacancy, and O^x_o is an O^{2-} anion on an oxygen site (neutral charge). The electric charges are defined with respect to the pure CeO_2 lattice. Eq. (7) shows that the higher the content of Gd_2O_3 is, the more oxygen vacancies are created. The content of Gd_2O_3 is 33 mol% in $Gd_2Ce_2O_7$, while that of Y_2O_3 is only 4.02 mol% in 8YSZ. Clearly, the concentration of oxygen vacancies in $Gd_2Ce_2O_7$ is significant higher than in 8YSZ. Therefore, the thermal conductivity of $Gd_2Ce_2O_7$ is lower than that of 8YSZ due to the scattering of the phonons by the oxygen vacancies.

In addition to the phonon scattering by the oxygen vacancies, another reason of low thermal conductivity of $Gd_2Ce_2O_7$ is the scattering of phonons by the substitutional cation. $Gd_2Ce_2O_7$ is a solid solute of Gd_2O_3 in CeO_2. For substitutional atoms existing in the lattice of oxides, the mean free path of phonon l_p is given by [27],

$$\frac{1}{l_p} = \frac{a^3}{4\pi v^4}\omega^4 c\left(\frac{\Delta M}{M}\right)^2 \tag{8}$$

where a^3 is the volume per atom, v the transverse wave speed, ω the phonon frequency, c the concentration per atom, M the average mass of the host atom, $M + \Delta M$ the average mass of the solute atom. Eq. (8) shows that the phonon mean free path is proportional to the square of the atomic weight difference between the solute and host (Ce) cations. Because atomic weight of Zr and Y are 91 and 89, respectively, the phonon scattering by Y^{3+} solute is negligible. On the other hand, the atomic weight of Cerium and gadolinium are 157.26 and 140, respectively, the effective phonon scattering induced by Gd^{3+} solute cations is significantly higher than that led by Y^{3+} solute cations, which contributes to the lower thermal conductivity of $Gd_2Ce_2O_7$.

It also can be noted from Fig. 6 that the thermal conductivity of $(Gd_{0.9}Ca_{0.1})_2Ce_2O_{6.9}$ is lower than that of $Gd_2Ce_2O_7$, the lower thermal conductivity of $(Gd_{0.9}Ca_{0.1})_2Ce_2O_{6.9}$ can also be ascribed to the scattering of phonons by the oxygen vacancies. It is well known that the substitutional solid solution is formed by the substitution of Gd^{3+} cation by bivalent cation when a bivalent oxide is doped into $Gd_2Ce_2O_7$. The substitution of two Gd^{3+} cations with two Ca^{2+} cations is accompanied by the incorporation of one oxygen vacancy, to maintain the electroneutrality of the lattice. The defect chemistry due to doping can be expressed using Kröger–Vink notation by the following equation,

$$2Gd^x_{Gd} + 2CaO \rightarrow Gd_2O_3 + 2Ca'_{Gd} + V''_o \tag{9}$$

where Ca'_{Gd} represents a Ca^{2+} cation that occupies a Gd^{3+} site. Eq. (9) shows that doping of Ca^{2+} introduces more oxygen vacancies, so the concentration of oxygen vacancies in $(Gd_{0.9}Ca_{0.1})_2Ce_2O_{6.9}$ is greater than that in $Gd_2Ce_2O_7$, which contributes to the lower ther-

mal conductivity of $(Gd_{0.9}Ca_{0.1})_2Ce_2O_{6.9}$ than that of $Gd_2Ce_2O_7$. In addition, the atomic weights of Ca and Gd are 40 and 157.26, difference in atomic weight also contributes lower thermal conductivity of $(Gd_{0.9}Ca_{0.1})_2Ce_2O_{6.9}$.

It is well known that low thermal conductivity is one of the most critical requirements for TBC. A good TBC material should have a much lower thermal conductivity [28]. The lower thermal conductivity of $Gd_2Ce_2O_7$ and $(Gd_{0.9}Ca_{0.1})_2Ce_2O_{6.9}$ in the temperature range between ambient and 800 °C indicates that these ceramic materials can be explored as novel candidate prospective ceramic materials for use in TBCs.

4. Conclusions

(1) Single phase $Gd_2Ce_2O_7$ and $(Gd_{0.9}Ca_{0.1})_2Ce_2O_{6.9}$ with fluorite structures were synthesized by solid state reaction methods between Gd_2O_3, CeO_2 and CaO powders at 1600 °C for 10 h.
(2) The lower thermal conductivities of $Gd_2Ce_2O_7$ and $(Gd_{0.9}Ca_{0.1})_2Ce_2O_{6.9}$ can be attributed to the significantly higher concentration of oxygen vacancies and the significantly larger atomic weight of the solute cations in these two ceramic materials.
(3) $Gd_2Ce_2O_7$ and $(Gd_{0.9}Ca_{0.1})_2Ce_2O_{6.9}$ can be explored as novel candidate ceramic materials for use in thermal barrier coatings.

Acknowledgements

This work is supported by the Doctor Research Fund of Henan Institute of Engineering (D2007012), and the program for innovative Research Team in Science and Technology in Henan Institute of Engineering (2009IRTHNIE05).

References

[1] N.P. Padture, M. Gell, E.H. Jordan, Science 4 (2003) 280.
[2] M. Matsumoto, J. Ceram. Soc. Jpn. 115 (2007) 118.
[3] X.Q. Cao, R. Vassen, D. Stover, J. Eur. Ceram. Soc. 24 (2004) 1.
[4] E.R. Andrievskaya, J. Eur. Ceram. Soc. 28 (2008) 2363.
[5] X. Huang, A. Zakurdaev, D. Wang, J. Mater. Sci. 43 (2008) 2631.
[6] D. Zhu, R.A. Miller, Int. J. Ceram. Technol. 1 (2004) 86.
[7] J. Wu, X.Z. Wei, N.P. Padture, P.G. Klemens, M. Gell, E. Garcia, J. Am. Ceram. Soc. 85 (2002) 3031.
[8] G. Suresh, G. Seenivasan, M.V. Krishnaiah, J. Alloys Compd. 269 (1998) 9.
[9] Q. Xu, W. Pan, J.D. Wang, L.H. Qi, H.Z. Miao, T. Kazutaka, Tortigoe, Mater. Lett. 59 (2005) 2804.
[10] D. Hui, Z.X. Hua, L.J. Yan, Z.Y. Fei, M. Jian, C.X. Qiang, Mater. Sci. Eng. A433 (2006) 1.
[11] J. Wang, S.X. Bai, H. Zhang, C.R. Zhang, J. Alloys Compd. 476 (2009) 89.
[12] Z.G. Liu, J.H. Ouyang, Y. Zhou, J. Li, X.L. Xia, J. Eur. Ceram. Soc. 29 (2009) 647.
[13] H.S. Zhang, Q. Xu, F.C. Wang, L. Liu, Y. Wei, X.G. Chen, J. Alloys Compd. 475 (2009) 624.
[14] H.S. Zhang, K. Sun, Q. Xu, F.C. Wang, L. Liu, J. Rare Earth 27 (2009) 222.
[15] Z.H. Xu, L.M. He, X.H. Zhong, R.D. Mu, S.M. He, X.Q. Cao, J. Alloys Compd. 478 (2009) 168.
[16] H.F. Chen, Y.F. Gao, S.Y. Tao, Y. Liu, H.J. Luo, J. Alloys Compd. 486 (2009) 391.
[17] Z.H. Xu, L.M. He, R.D. Mu, G.H. Huang, X.Q. Cao, Appl. Surf. Sci. 256 (2010) 3661.
[18] C.X. Qiang, R. Vassen, W. Fischer, F. Tietz, D. Stover, Adv. Mater. 9 (2003) 1438.
[19] H. Dai, X.H. Zhong, J.Y. Li, J. Meng, X.Q. Cao, Surf. Coat. Technol. 201 (2006) 2527.
[20] S.J. Patwe, B.R. Ambekar, A.K. Tyagi, J. Alloys Compd. 389 (2005) 243.
[21] P.G. Spencer, Thermochem. Acta 314 (1999) 1.
[22] J.D. Leitner, P. Chuchvalec, D. Sedmidubsky, Thermochim. Acta 395 (2003) 27.
[23] M.A. Subramanian, G. Aravamudan, G.V.S. Rao, Prog. Solid State Chem. 15 (1983) 55.
[24] X.L. Xia, J.H. Ouyang, Z.G. Liu, J. Power Sources 189 (2009) 888.
[25] Z.G. Liu, J.H. Ouyang, Y. Zhou, J. Mater. Sci. 43 (2008) 3596.
[26] J.R. Nicholls, K.J. Lawson, A. Johnstone, D.S. Rickerby, Surf. Coat. Technol. 151–152 (2002) 383.
[27] X. Qiang, P. Wei, W.J. Dong, Q.L. Hao, M.H. Zhou, Mater. Lett. 59 (2005) 2804.
[28] S. Yamanaka, T. Maekawa, H. Muta, T. Matsuda, S. Kobayshi, K. Kurosaki, J. Alloys Compd. 381 (2004) 295.